ACS APPLIED MATERIALS & INTERFACES

Research Article

www.acsami.org

Boosting Catalytic Performance of Metal–Organic Framework by Increasing the Defects via a Facile and Green Approach

Gan Ye,[†] Dan Zhang,[†] Xiangfu Li,[‡] Kunyue Leng,[†] Wenjuan Zhang,[‡] Jun Ma,[‡] Yinyong Sun,*[,†] Wei Xu,[§] and Shengqian Ma*[,∥]

[†]MIIT Key Laboratory of Critical Materials Technology for New Energy Conversion and Storage, School of Chemistry and Chemical Engineering, and [‡]School of Municipal and Environmental Engineering, Harbin Institute of Technology, Harbin, 150001, China

[§]State Key Lab of Inorganic Synthesis and Preparative Chemistry, College of Chemistry, Jilin University, Changchun, 130012, China

[∥]Department of Chemistry, University of South Florida, 4202 Easter Fowler Avenue, Tampa, Florida 33620, United States

Supporting Information

ABSTRACT: The control of defects in crystalline materials has long been of significance since the defects are correlated with the performances of the materials. Yet such control remains a challenge for metal–organic frameworks (MOFs), which are usually well-crystallized under hydro-/solvothermal conditions. In this contribution, we demonstrate for the first time how to increase the defects of MOF via a facile and green approach as exemplified in the context of solvent-free synthesis of UiO–66(Zr). Such increase of defects leads to drastic enhancement of catalysis performance when compared to UiO–66(Zr) prepared from conventional hydro-/solvothermal synthesis. Our work therefore not only opens a new door for boosting the catalytic activities of MOFs but also contributes a new approach to control the defects in crystalline materials for various applications.

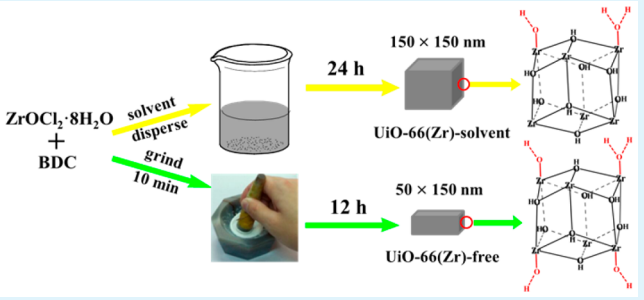

KEYWORDS: *UiO–66(Zr), defect sites, solvent-free, oxidation, desulfurization*

1. INTRODUCTION

The formation of defects within crystalline materials is of great significance because the defects are profoundly correlated with the performances of the materials involving electricity, optics, magnetics, and catalysis.[1−8] Emerging as a new class of crystalline materials, metal–organic frameworks (MOFs) have received considerable attention in recent years due to their potential for a variety of applications such as gas storage, separation, biomedicine, and heterogeneous catalysis.[9−13] Recently, there is an escalating interest in the characterization and introduction of defects within MOFs.[14−17] For example, UiO–66(Zr) with exceptional thermal, mechanical and chemical stability and high surface area, has been widely investigated.[18−21] It has been found that the defects within UiO–66(Zr) can be formed when either 1 linker or an entire zirconium cluster associated with 12 linkers is missing from the framework, and the missing linker is replaced by hydroxide or water (M–OH and M–OH_2) as terminal ligand at the nodes.[22−25]

On the other hand, as for the synthesis of UiO–66(Zr) with defects, the addition of a modulator, typically a monocarboxylic acid, was usually required.[26−32] For examples, Zhou and co-workers reported that the missing linker can be produced by varying the concentration of acetic acid modulator and the synthetic temperature.[33] De Vos and co-workers showed that the addition of trifluoroacetic acid during the synthesis is helpful for the formation of defect sites.[34] Although some works have been done about the introduction of defects into MOFs, the addition of monocarboxylic acid and solvent are the prerequisite in those synthetic systems.[35−39] This would essentially bring about an environmental problem and an increase in preparation costs when it is scaled up. Thus, there is a need to develop facile and green approaches to prepare such materials.[40−42]

In this work, we report that MOFs with defects can be synthesized via a facile and green route. Here, UiO–66(Zr) was used as an example to testify to the efficiency of this synthetic strategy.[43,44]

2. EXPERIMENTAL SECTION

2.1. Materials. Zirconyl chloride octahydrate ($ZrOCl_2·8H_2O$), zirconium tetrachloride ($ZrCl_4$), zirconium nitrate pentahydrate ($Zr(NO_3)_4·5H_2O$), 1,4-benzenedicarboxylic acid (BDC), $NaNO_3$, NaOH, *N*,*N*′-dimenthylformamide (DMF), hydrochloric acid (HCl 37%), hydrogen peroxide (30 wt %), cumene hydroperoxide (70%), ethanol, acetonitrile, phenethyl alcohol, and *n*-octane were purchased from Sinopharm Chemical Reagent Co. Dibenzothiophene (DBT) and 4,6-dimethyldibenzothiophene (4,6-DMDBT) were purchased

Received: July 15, 2017
Accepted: September 18, 2017
Published: September 18, 2017

DOI: 10.1021/acsami.7b10337
ACS Appl. Mater. Interfaces 2017, 9, 34937−34943

from Aldrich. All chemicals and solvents are analytical purity and used without further purification.

2.2. Synthesis of Materials. *2.2.1. Synthesis of UiO−66(Zr)-Free.* In a typical synthesis, $ZrOCl_2·8H_2O$ (1.5 mmol) and BDC (1.5 mmol) were mixed and ground in a mortar by hand for about 10 min at room temperature. Then the obtained materials were transferred into an autoclave and crystallized at a certain temperature and time. After cooling to room temperature, the resulting white solid was washed with 70 °C ethanol and dried under vacuum for 12 h at 150 °C.

2.2.2. Synthesis of UiO−66(Zr)-Solvent. UiO−66(Zr)-solvent was prepared according to the reported procedure.[45]

2.2.3. Synthesis of UiO−66(Zr) without Defects. UiO−66(Zr) without defects was synthesized according to the reported procedure.[36]

2.3. Characterization. Powder X-ray diffraction (XRD) patterns were recorded on a Rigaku D/Max-2550 diffractometer equipped with a SolX detector-Cu Kα radiation with wavelength of λ = 1.5418 Å. Nitrogen sorption isotherms were obtained at 77 K on a 3H-2000PS1 gas sorption and porosimetry system. Samples were normally prepared for measurement after degassing at 423 K under vacuum until a final pressure of 1×10^{-3} Torr was reached. Scanning electron microscopy (SEM) images and energy dispersive X-ray spectroscopy (EDX) elemental mapping were recorded on SUPRA 55 operated with an acceleration voltage of 200 kV. Zr content was determined by inductively coupled plasma emission spectrometry (ICP) on a PerkinElmer Optima 5300DV atomic emission spectrometer. Fourier Transform infrared (FT-IR) spectra were recorded on a NicoLET iS10 spectrometer. Thermogravimetric analysis was carried out on TGA Q500 from TA company. Potentiometric acid−base titrations were completed with a Metrohm Titrando 905 autotitrator equipped with Dosino 800 20 and 10 mL dosing units.

2.4. Catalytic Tests. The oxidative desulfurization (ODS) reaction was performed using a liquid−liquid extraction and the oxidative catalytic desulfurization stage. A certain amount of DBT or DMDBT were dissolved in *n*-octane (with a concentration of 1000 or 500 ppmw of sulfur from DBT or DMDBT) to act as model fuel. The reactions were performed under air in a closed 100 mL three-neck glass flask with a vigorous magnetic stirrer (1000 r/min) and immersed in an oil bath at 60 °C. In a standard run, the catalyst (50 mg) was added to model fuel (10 g) and acetonitrile (10 g), and the resulting mixture was stirred for 10 min at 60 °C. The catalytic reaction process is initiated by the addition of H_2O_2 (30 wt %, 195 μL) as oxidant with a H_2O_2/S molar ratio of 6:1. The agitation of reaction solution was stopped under different times until the liquids layered. Then the right amount of liquid in the octane phase was taken and analyzed by gas chromatography on an Agilent 7890A GC with an FID detector using a 30 m packed HP5 column. The products were also identified by GC-MS (5975C-7890A) analysis. The removal content of DBT or DMDBT was calculated according to the equation $R = (1 - C_t/C_0) \times 100\%$, where C_0 and C_t stand for the initial concentration and the reaction concentration of DBT or DMDBT in *n*-octane phase after *t* minutes, respectively.

The oxidation reaction of benzyl alcohol was performed in a 100 mL round-bottom flask equipped with a condenser and a magnetic stirrer bar. In a typical experiment, 1.0 mmol of benzyl alcohol, 10 mL of CH_3CN, and 50 mg of activated catalyst were used. After the above solution was maintained at 80 °C for 15 min, 1 mL of H_2O_2 (30%, 10 mmol) was added to the mixture. This moment was regarded as initial reaction time. Liquid samples were withdrawn at regular intervals and analyzed by gas chromatography on an Agilent 7890A GC with FID detector using a 30 m packed HP5 column.

3. RESULTS AND DISCUSSION

Specifically, the synthetic route to prepare UiO−66(Zr) with increasing defects without the addition of monocarboxylic acid and solvent is shown in Scheme 1. This process may be finished in a relatively short crystalline time (less than 12 h) with high yield, low preparation cost, and good reproducibility. Typically, $ZrOCl_2·8H_2O$ and 1,4-benzene dicarboxylate (BDC) were mixed and ground about 10 min at room temperature. Then the obtained materials were transferred into an autoclave and crystallized at a certain temperature. The detailed synthetic procedures are shown in the Supporting Information. After the optimization of some synthetic parameters (Table S1), a representative sample named as UiO−66(Zr)-free was prepared at 130 °C in a crystalline time of 12 h and was selected. For comparison, conventional UiO−66(Zr) was synthesized with the addition of solvent according to the reported procedures.[45] The resultant sample was labeled as UiO−66(Zr)-solvent. As shown in Figure 1, the powder XRD patterns of UiO−66(Zr)-free and UiO−66(Zr)-solvent exhibited well-resolved diffraction peaks corresponding to calculated ones, which are characteristic of the UiO−66(Zr) structure. No additional peaks were observed, indicating that no impure crystalline phases were formed.

Scheme 1. Imaginative Diagram about Synthetic Process of UiO−66(Zr) under Different Conditions

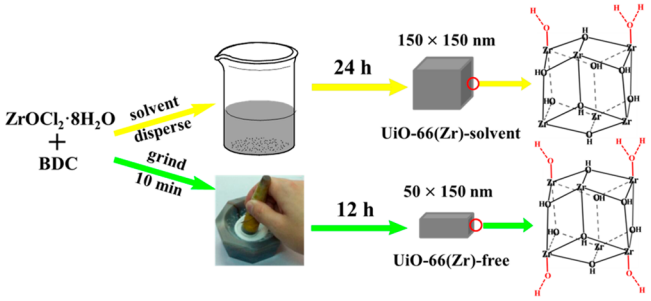

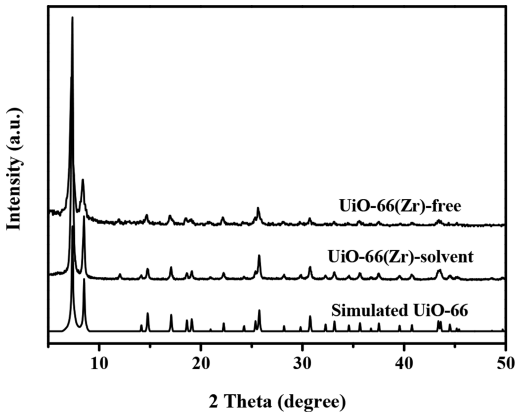

Figure 1. XRD patterns of various samples.

The SEM images of UiO−66(Zr)-solvent and UiO−66(Zr)-free are shown in Figure 2. Obviously, both samples displayed different morphologies and crystal sizes. UiO−66(Zr)-solvent had a morphology of a cubiclike shape and was mainly composed of crystals with a size around 150 × 150 nm (Figure 2a,b). Comparatively, UiO−66(Zr)-free exhibited a morphology of flakelike shape and smaller crystal size (about 50 × 150 nm) than UiO−66(Zr)-solvent (Figure 2c,d). These results indicated that the synthetic method had a great influence on the morphology and crystal size of formed UiO−66(Zr) materials.

N_2 sorption isotherms of samples were shown in Figure 3. Both UiO−66(Zr)-free and UiO−66(Zr)-solvent exhibited type I isotherm in the region of low relative pressure, indicating the existence of micropores. Further, the pore distribution curve of UiO−66(Zr)-free gave two types of pores centered

DOI: 10.1021/acsami.7b10337
ACS Appl. Mater. Interfaces 2017, 9, 34937−34943

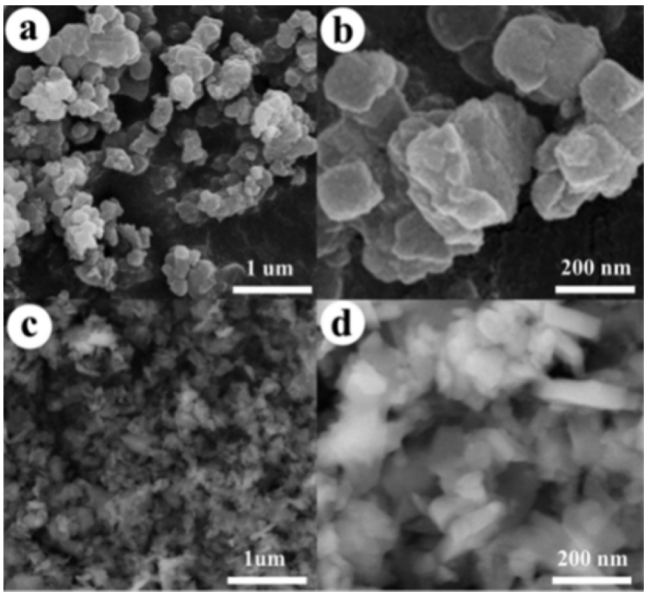

Figure 2. SEM images of UiO−66(Zr)-solvent (a and b) and UiO−66(Zr)-free (c and d).

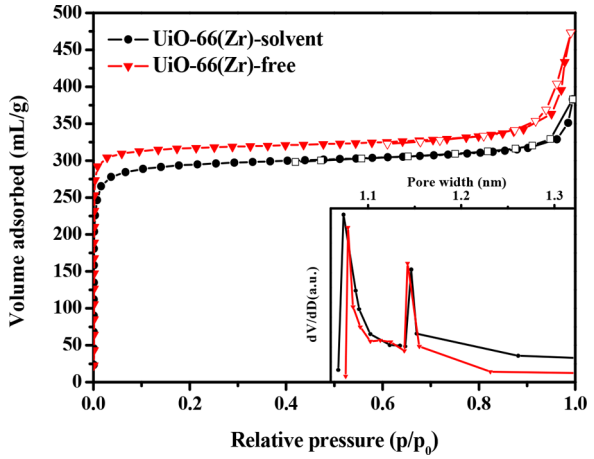

Figure 3. N_2 sorption isotherms and pore distribution curves of various samples.

around 1.07 and 1.15 nm, which are similar to those of UiO−66(Zr)-solvent (Figure 3 inset). The detailed sorption data are listed in Table 1. UiO−66(Zr)-free possessed higher surface area and pore volume than UiO−66(Zr)-solvent, suggesting that defect sites in the structure of UiO−66(Zr)-free might be formed.

Table 1. Textural Properties and Yield of Various Samples

samples	Zr content[a] (wt %)	BET surface area (m^2/g)	micropore volume[b] (mL/g)	total pore volume (mL/g)	yield[c] (%)
UiO−66(Zr)-solvent	31.4	1000	0.43	0.60	45.4
UiO−66(Zr)-free	32.2	1115	0.48	1.15	92.1

[a]Measured by ICP. [b]HK method. [c]Calculated by the additional amount of BDC.

The results from thermogravimetric analysis indicated that UiO−66(Zr)-free had high thermal stability like UiO−66(Zr)-solvent (Figure S1). Two weight losses can be observed. The first one before 400 °C can be attributed to the removal of guest molecules like water or DMF. The second one from 400 to 550 °C should result from the decomposition of the framework. The amount of second loss (40 wt %) for UiO−66(Zr)-free was near that for UiO−66(Zr)-solvent, suggesting that BDC content in the framework of both samples should be close because their Zr content was similar (Table 1). Differently, the first weight loss in UiO−66(Zr)-free was higher than that in UiO−66(Zr)-solvent. Considering that no DMF was added during the synthesis of UiO−66(Zr)-free, this loss should be attributed to the removal of adsorption water with different sites, suggesting that different defect sites were possibly formed in the structure of UiO−66(Zr)-free. It need be noted that the adsorption water possibly originated from crystal water in Zr precursors during synthesis, although water was not added. Comparatively, that loss in UiO−66(Zr)-solvent possibly resulted from DMF and water. This fact can be proved by FT-IR spectroscopy. UiO−66(Zr)-solvent displayed a strong absorption band at 1657 cm^{-1} assigned to the stretching vibration of the C═O bond from DMF and this absorption band disappeared in UiO−66(Zr)-free (Figure S2). In addition, it is known that the wavenumber separation between the absorption bands around 1400 and 1500−1700 cm^{-1} can give more information on coordination modes of BDC to Zr. The splitting is larger than 200 cm^{-1} when BDC acts as a monodentate ligand and in the range of 50−150 cm^{-1}, if it acts as a bidentate ligand. A splitting of 130−200 cm^{-1} is considered as bridging ligands.[46,47] It can be seen from Figure S2 that there is a strong splitting of 187 cm^{-1} with a weak one of 106 cm^{-1} for UiO−66(Zr)-free and UiO−66(Zr)-solvent. The results indicated that the coordination modes of BDC in UiO−66(Zr)-free and UiO−66(Zr)-solvent mainly consisted of bridging ligands with a small amount of bidentate liagands.

As known, acid−base titration method was demonstrated to be an efficient approach to characterize defect sites in MOFs materials.[48−50] Here, the acid−base titration curves of both samples were measured to detect the situation of defect sites in UiO−66(Zr). As shown in Figure 4, both UiO−66(Zr)-solvent and UiO−66(Zr)-free displayed the titration curves with three apparent inflection points, which should correspond to three types of protons (μ_3-OH, Zr−OH_2, and Zr−OH).[38,48] The first-derivative curves were fit to Lorentzian-type peaks for determining the equivalence points in the titration curves. The first pK_a value can be assigned to the μ_3-OH proton. The other titratable protons corresponded to defect sites in the node. The second one is the Zr−OH_2 proton and the third one is the Zr−OH proton. On the basis of the calculation, UiO−66(Zr)-solvent gave a missing linker number of 1.53 in the structure. Comparatively, the number of missing linkers in UiO−66(Zr)-free reached 2.16, which is even higher than those in some reported UiO−66(Zr) materials with defect sites prepared by the addition of monocarboxylic acid. Furthermore, it can be noted from the calculation results that those defect sites in UiO−66(Zr)-free mainly consisted of Zr−OH sites. Such defect sites could be highly active for some catalytic oxidative reactions.

To verify the role of defect sites, the oxidative desulfurization (ODS) reactions of dibenzothiophene (DBT) and 4,6-dimethyl-dibenzothiophene (4,6-DMDBT) were first carried out (Scheme S1).[51−53] As seen in Figure 5, the reaction cannot

DOI: 10.1021/acsami.7b10337
ACS Appl. Mater. Interfaces 2017, 9, 34937−34943

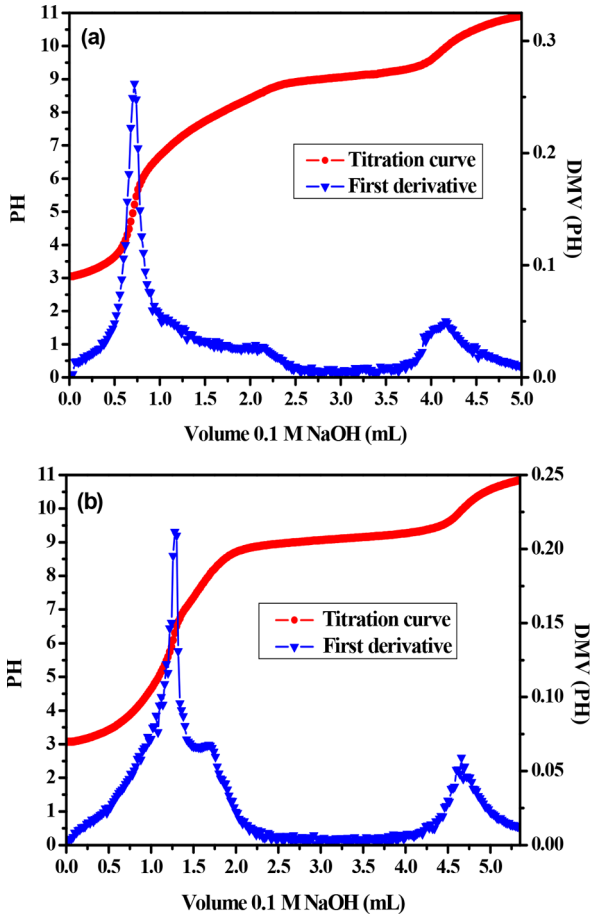

Figure 4. Acid−base titration curve and first derivative curve for UiO−66(Zr)-solvent (a) and UiO−66(Zr)-free (b).

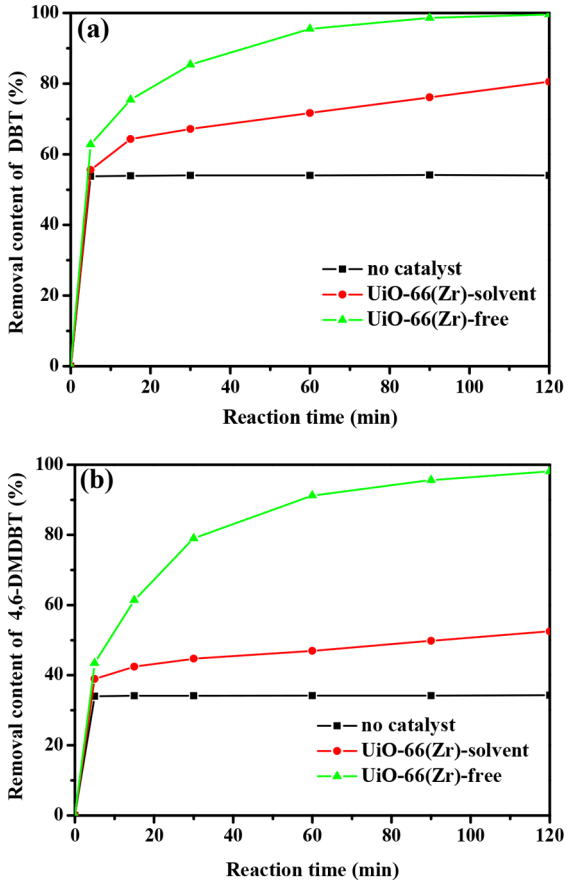

Figure 5. Removal content of DBT (a) and 4,6-DMDBT (b) with reaction time over various catalysts.

occur if no catalyst was added. When UiO−66(Zr)-solvent was used as catalyst, only 80.5% DBT can be removed after a reaction time of 120 min. In comparison, the removal content of DBT over UiO−66(Zr)-free may reach 99.6% under the same reaction time. Such superior catalytic performance over UiO−66(Zr)-free can also be demonstrated when cumene hydroperoxide was used as oxidant without the addition of acetonitrile (Figure S3). More importantly, UiO−66(Zr)-free showed superior ODS performance for the removal of 4,6-DMDBT with large molecular size. The removal content of 4,6-DMDBT over UiO−66(Zr)-free reached 98.1% after 120 min (Figure 5b), which was twice higher than that over UiO−66(Zr)-solvent (52.5%). These results indicated that UiO−66(Zr)-free had potential applications in the field of deep oxidative desulfurization of fuel oil.

To further demonstrate the effect of defects, the catalytic performance of UiO−66(Zr) without defects was evaluated by ODS of DBT. Clearly, UiO−66(Zr) without defects was almost inactive in the reaction (Figure S4). Additionally, the oxidation of benzyl alchol was also studied (Scheme S2). UiO−66(Zr)-free still showed higher catalytic activity than UiO−66(Zr)-solvent (Figure S5). These results proved fully that defect sites in UiO−66(Zr)-free played a positive role in enhancing the catalytic performance.

On the basis of this fact that UiO−66(Zr)-free gave enhanced performance, its reusability was evaluated in the context of ODS of DBT. After each cycle, the catalyst was recovered by centrifugation, was washed with acetonitrile, and reused in the next cycle under the same reaction conditions. As shown in Figure 6, UiO−66(Zr)-free almost maintained the initial activity after four cycles (above 99% DBT conversion). These results highlight the heterogeneous and reusable nature of UiO−66(Zr)-free.

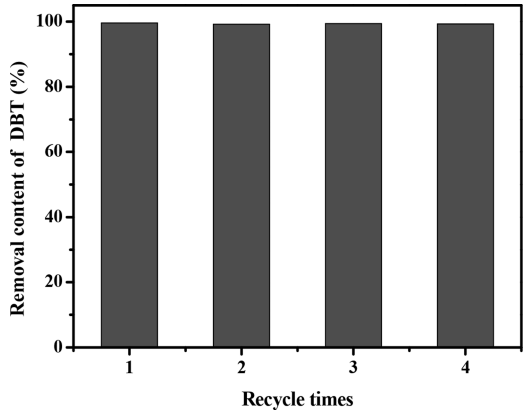

Figure 6. Reusability of UiO−66(Zr)-free in the ODS reaction of DBT.

In addition to the effect of some synthetic parameters including crystallization temperature and time, metal precursor was also investigated during the preparation of UiO−66(Zr)-free. Apparently, the structure of UiO−66(Zr)-free can be formed when the crystallization temperature was tuned in the range of 100−180 °C (Figures S6 and S7). Accordingly, BET

DOI: 10.1021/acsami.7b10337
ACS Appl. Mater. Interfaces 2017, 9, 34937−34943

surface area of the obtained samples was changed in the range of 881−1187 m^2/g (Figure S8, Table S1). It can be noted that higher crystallization temperature (above 130 °C) easily resulted in the formation of the materials with lower surface area. Interestingly, shortening the crystalline time to 6 h can still produce UiO−66(Zr) with a high surface area of 1095 m^2/g (Figure S9, Table S1), suggesting that such synthetic approach can seemly accelerate the crystallization of UiO−66(Zr) structure. Importantly, the yield of UiO−66(Zr) materials prepared by this method in most cases can reach above 90% (Table S1), which is nearly twice as that of UiO−66(Zr)-solvent. Moreover, the type of Zr source also played a vital role in the formation of UiO−66(Zr). If $ZrOCl_2·8H_2O$ was replaced by $ZrCl_4$ or $Zr(NO_3)_4·5H_2O$ during this synthesis, only white solid powders with lower BET surface area (19−68 m^2/g) were obtained. This result suggested that Zr source like $ZrOCl_2·8H_2O$ possibly contributed to the formation of Zr−O clusters in UiO−66(Zr) structure. Further, to investigate the formation process of UiO−66(Zr) before and after crystallization, the XRD patterns of $ZrOCl_2·8H_2O$, BDC, physical mix and grinding of $ZrOCl_2·8H_2O$ and BDC, and UiO−66(Zr) are shown in Figure S10. Clearly, after grinding, the intensity of the diffraction peak assigned to BDC turned weak, revealing that the interaction of $ZrOCl_2·8H_2O$ and BDC occurred. Possibly, this process supplied the driving force for the next crystallization.

4. CONCLUSIONS

In summary, UiO−66(Zr) with increasing defects has been successfully synthesized without the addition of monocarboxylic acid and solvent. The number of missing linkers per $Zr_6O_4(OH)_4(BDC)_6$ in this material reached 2.16, which is much higher than that in UiO−66(Zr) prepared by a conventional method. As a result, this material exhibited enhanced catalytic activity in a series of catalytic oxidative reactions including the ODS reactions of DBT and 4,6-DMDBT and oxidation of benzyl alcohol. Additionally, such synthetic method is green and facile, which can produce UiO−66(Zr) material with high yield and low cost. Because of the simplification, rapidness, high yield, low cost, and environmental benignancy of synthetic procedures, it will be of great significance for potential applications.

■ ASSOCIATED CONTENT

Supporting Information

The Supporting Information is available free of charge on the ACS Publications website at DOI: 10.1021/acsami.7b10337.

Potentiometric acid−base titrations and calculation of the number of defect sites of UiO−66-free and UiO−66-solvent, the detailed synthetic procedures of various samples, the scheme of oxidation of DBT, DMDBT, and benzyl alcohol, TGA curves and FT-IR spectra of UiO−66(Zr)-solvent and UiO−66(Zr)-free, ODS of DBT curves over UiO−66(Zr) without defects, oxidation of benzyl alcohol curves of UiO−66(Zr)-solvent and UiO−66(Zr)-free, XRD patterns of various samples, and N_2 sorption isotherms curves of various samples (PDF)

■ AUTHOR INFORMATION

Corresponding Authors

*E-mail: yysun@hit.edu.cn.
*E-mail: sqma@usf.edu.

ORCID

Yinyong Sun: 0000-0002-5570-5089
Shengqian Ma: 0000-0002-1897-7069

Author Contributions

The manuscript was written through contributions of all authors. All authors have given approval to the final version of the manuscript.

Notes

The authors declare no competing financial interest.

■ ACKNOWLEDGMENTS

The authors acknowledge the financial support from the Fundamental Research Funds for the Central Universities (Grant No. HIT. NSRIF. 2015046), Open Funding from the State Key Lab of Inorganic Synthesis and Preparative Chemistry, Jilin University, and Key Laboratory of Functional Inorganic Material Chemistry (Heilongjiang University), Ministry of Education.

■ REFERENCES

(1) Yaghi, O. M.; O'Keeffe, M.; Ockwig, N. W.; Chae, H. K.; Eddaoudi, M.; Kim, J. Reticular Synthesis and the Design of New Materials. *Nature* **2003**, *423*, 705−714.

(2) Lee, J. Y.; Farha, O. K.; Roberts, J.; Scheidt, K. A.; Nguyen, S. T.; Hupp, J. T. Metal-Organic Framework Materials as Catalysts. *Chem. Soc. Rev.* **2009**, *38*, 1450−1459.

(3) Li, J. R.; Kuppler, R. J.; Zhou, H. C. Selective Gas Adsorption and Separation in Metal−Organic Frameworks. *Chem. Soc. Rev.* **2009**, *38*, 1477−1504.

(4) Sun, L.; Campbell, M. G.; Dincă, M. Electrically Conductive Porous Metal-Organic Frameworks. *Angew. Chem., Int. Ed.* **2016**, *55*, 3566−3579.

(5) Zeng, M. H.; Yin, Z.; Tan, Y. X.; Zhang, W. X.; He, Y. P.; Kurmoo, M. Nanoporous Cobalt(II) MOF Exhibiting Four Magnetic Ground States and Changes in Gas Sorption upon Post-Synthetic Modification. *J. Am. Chem. Soc.* **2014**, *136*, 4680−4688.

(6) Wang, C.; Volotskova, O.; Lu, K.; Ahmad, M.; Sun, C.; Xing, L.; Lin, W. Synergistic Assembly of Heavy Metal Clusters and Luminescent Organic Bridging Ligands in Metal-organic Frameworks for Highly Efficient X-ray Scintillation. *J. Am. Chem. Soc.* **2014**, *136*, 6171−6174.

(7) Corma, A.; García, H.; Llabrés i Xamena, F. X. Engineering Metal Organic Frameworks for Heterogeneous Catalysis. *Chem. Rev.* **2010**, *110*, 4606−4655.

(8) Bai, Y.; Dou, Y.; Xie, L. H.; Rutledge, W.; Li, J. R.; Zhou, H. C. Zr-Based Metal−Organic Frameworks: Design, Synthesis, Structure, and Applications. *Chem. Soc. Rev.* **2016**, *45*, 2327−2367.

(9) Sumida, K.; Rogow, D. L.; Mason, J. A.; McDonald, T. M.; Bloch, E. D.; Herm, Z. R.; Bae, T. H.; Long, J. R. Carbon Dioxide Capture in Metal-Organic Frameworks. *Chem. Rev.* **2012**, *112*, 724−781.

(10) Furukawa, H.; Gándara, F.; Zhang, Y. B.; Jiang, J.; Queen, W. L.; Hudson, M. R.; Yaghi, O. M. Water Adsorption in Porous Metal-Organic Frameworks and Related Materials. *J. Am. Chem. Soc.* **2014**, *136*, 4369−4381.

(11) Gamage, N. D. H.; McDonald, K. A.; Matzger, A. J. MOF-5-Polystyrene: Direct Production from Monomer, Improved Hydrolytic Stability, and Unique Guest Adsorption. *Angew. Chem., Int. Ed.* **2016**, *55*, 12099−12103.

(12) Yang, D.; Odoh, S. O.; Borycz, J.; Wang, T. C.; Farha, O. K.; Hupp, J. T.; Cramer, C. J.; Gagliardi, L.; Gates, B. C. Tuning Zr_6 Metal-Organic Framework (MOF) Nodes as Catalyst Supports: Site Densities and Electron-Donor Properties Influence Molecular Iridium Complexes as Ethylene Conversion Catalysts. *ACS Catal.* **2016**, *6*, 235−247.

(13) Dhakshinamoorthy, A.; Asiri, A. M.; García, H. Metal-Organic Framework (MOF) Compounds: Photocatalysts for Redox Reactions

DOI: 10.1021/acsami.7b10337
ACS Appl. Mater. Interfaces 2017, 9, 34937−34943

and Solar Fuel Production. *Angew. Chem., Int. Ed.* **2016**, *55*, 5414−5445.
(14) Cliffe, M. J.; Wan, W.; Zou, X. D.; Chater, P. A.; Kleppe, A. K.; Tucker, M. G.; Wilhelm, H.; Funnell, N. P.; Coudert, F. X.; Goodwin, A. L. Correlated Defect Nanoregions in a Metal-Organic Framework. *Nat. Commun.* **2014**, *5*, 4176.
(15) De Vos, A.; Hen-drickx, K.; Van Der Voort, P.; Van Speybroeck, V.; Lejaeghere, K. Missing Linkers: An Alternative Pathway to UiO-66 Electronic Structure Engineering. *Chem. Mater.* **2017**, *29*, 3006−3019.
(16) Taylor, J.; Dekura, S.; Ikeda, R.; Kitagawa, H. Defect Control To Enhance Proton Conductivity in a Metal-Organic Framework. *Chem. Mater.* **2015**, *27*, 2286−2289.
(17) Zhao, Y. J.; Zhang, Q.; Li, Y. L.; Zhang, R.; Lu, G. Large-Scale Synthesis of Monodisperse UiO-66 Crystals with Tunable Sizes and Missing Linker Defects via Acid/Base Co-Modulation. *ACS Appl. Mater. Interfaces* **2017**, *9*, 15079−15085.
(18) Shearer, G. C.; Forselv, S.; Chavan, S.; Bordiga, S.; Mathisen, K.; Bjørgen, M.; Svelle, S.; Lillerud, K. P. In Situ Infrared Spectroscopic and Gravimetric Characterisation of the Solvent Removal and Dehydroxylation of the Metal Organic Frameworks UiO-66 and UiO-67. *Top. Catal.* **2013**, *56*, 770−782.
(19) Valenzano, L.; Civalleri, B.; Chavan, S.; Bordiga, S.; Nilsen, M. H.; Jakobsen, S.; Lillerud, K. P.; Lamberti, C. Disclosing the Complex Structure of UiO-66 Metal Organic Framework: A Synergic Combination of Experiment and Theory. *Chem. Mater.* **2011**, *23*, 1700−1718.
(20) Wang, P.; Feng, J.; Zhao, Y. P.; Wang, S. B.; Liu, J. MOF-Derived Tungstated Zirconia as Strong Solid Acids toward High Catalytic Performance for Acetalization. *ACS Appl. Mater. Interfaces* **2016**, *8*, 23755−23762.
(21) Wang, X. S.; Li, L.; Liang, J.; Huang, Y. B.; Cao, R. Boosting Oxidative Desulfurization of Model and Real Gasoline over Phosphotungstic Acid Encapsulated in Metal−Organic Frameworks: The Window Size Matters. *ChemCatChem* **2017**, *9*, 971−979.
(22) Katz, M. J.; Klet, R. C.; Moon, S. Y.; Mondloch, J. E.; Hupp, J. T.; Farha, O. K. One Step Backward Is Two Steps Forward: Enhancing the Hydrolysis Rate of UiO-66 by Decreasing [OH^-]. *ACS Catal.* **2015**, *5*, 4637−4642.
(23) Ghosh, P.; Colón, Y.; Snurr, R. Q. Water Adsorption in UiO-66: The Importance of Defects. *Chem. Commun.* **2014**, *50*, 11329−11331.
(24) Vandichel, M.; Hajek, J.; Vermoortele, F.; Waroquier, M.; De Vos, D. E.; Van Speybroeck, V. Active Site Engineering in UiO-66 Type Metal-Organic Frameworks by Intentional Creation of Defects: A Theoretical Rationalization. *CrystEngComm* **2015**, *17*, 395−406.
(25) Canivet, J.; Vandichel, M.; Farrusseng, D. Origin of Highly Active Metal-Organic Framework Catalysts: Defects? Defects! *Dalton Trans.* **2016**, *45*, 4090−4099.
(26) Ragon, F.; Horcajada, P.; Chevreau, H.; Hwang, Y. K.; Lee, U. H.; Miller, S. R.; Devic, T.; Chang, J. S.; Serre, C. In Situ Energy-Dispersive X-ray Diffraction for the Synthesis Optimization and Scale-up of the Porous Zirconium Terephthalate UiO-66. *Inorg. Chem.* **2014**, *53*, 2491−2500.
(27) Ren, J. W.; Langmi, H. W.; North, B. C.; Mathe, M.; Bessarabov, D. Modulated Synthesis of Zirconium-Metal Organic Framework (Zr-MOF) for Hydrogen Storage Applications. *Int. J. Hydrogen Energy* **2014**, *39*, 890−895.
(28) Van de Voorde, B.; Stassen, I.; Bueken, B.; Vermoortele, F.; De Vos, D.; Ameloot, R.; Tan, J. C.; Bennett, T. D. Improving the Mechanical Stability of Zirconium-Based Metal-Organic Frameworks by Incorporation of Acidic Modulators. *J. Mater. Chem. A* **2015**, *3*, 1737−1742.
(29) Ma, J. L.; Wong-Foy, A. G.; Matzger, A. J. The Role of Modulators in Controlling Layer Spacings in a Tritopic Linker Based Zirconium 2D Microporous Coordination Polymer. *Inorg. Chem.* **2015**, *54*, 4591−4593.
(30) Zahn, G.; Schulze, H. A.; Lippke, J.; König, S.; Sazama, U.; Fröba, M.; Behrens, P. A water-Born Zr-Based Porous Coordination Polymer: Modulated Synthesis of Zr-Fumarate MOF. *Microporous Mesoporous Mater.* **2015**, *203*, 186−194.
(31) Schaate, A.; Roy, P.; Godt, A.; Lippke, J.; Waltz, F.; Wiebcke, M.; Behrens, P. Modulated Synthesis of Zr-Based Metal-Organic Frameworks: From Nano to Single Crystals. *Chem. - Eur. J.* **2011**, *17*, 6643−6651.
(32) Hu, Z. G.; Castano, I.; Wang, S. N.; Wang, Y. X.; Peng, Y. W.; Qian, Y. H.; Chi, C. L.; Wang, X. R.; Zhao, D. Modulator Effects on the Water-Based Synthesis of Zr/Hf Metal-Organic Frameworks: Quantitative Relationship Studies between Modulator, Synthetic Condition, and Performance. *Cryst. Growth Des.* **2016**, *16*, 2295−2301.
(33) Wu, H.; Chua, Y. S.; Krungleviciute, V.; Tyagi, M.; Chen, P.; Yildirim, T.; Zhou, W. Unusual and Highly Tunable Missing-Linker Defects in Zirconium Metal-Organic Framework UiO-66 and Their Important Effects on Gas Adsorption. *J. Am. Chem. Soc.* **2013**, *135*, 10525−10532.
(34) Vermoortele, F.; Bueken, B.; Le Bars, G.; Van de Voorde, B.; Vandichel, M.; Houthoofd, K.; Vimont, A.; Daturi, M.; Waroquier, M.; Van Speybroeck, V. V.; Kirschhock, C.; De Vos, D. E. Synthesis Modulation as a Tool To Increase the Catalytic Activity of Metal-Organic Frameworks: The Unique Case of UiO-66(Zr). *J. Am. Chem. Soc.* **2013**, *135*, 11465−11468.
(35) Shearer, G. C.; Chavan, S.; Ethiraj, J.; Vitillo, J. G.; Svelle, S.; Olsbye, U.; Lamberti, C.; Bordiga, S.; Lillerud, K. P. Tuned to Perfection: Ironing Out the Defects in Metal−Organic Framework UiO-66. *Chem. Mater.* **2014**, *26*, 4068−4071.
(36) Shearer, G. C.; Chavan, S.; Bordiga, S.; Svelle, S.; Olsbye, U.; Lillerud, K. P. Defect Engineering: Tuning the Porosity and Composition of the Metal-Organic Framework UiO-66 via Modulated Synthesis. *Chem. Mater.* **2016**, *28*, 3749−3761.
(37) Shearer, G. C.; Vitillo, J. G.; Bordiga, S.; Svelle, S.; Olsbye, U.; Lillerud, K. P. Functionalizing the Defects: Postsynthetic Ligand Exchange in the Metal Organic Framework UiO-66. *Chem. Mater.* **2016**, *28*, 7190−7193.
(38) DeStefano, M. R.; Islamoglu, T.; Garibay, S. J.; Hupp, J. T.; Farha, O. K. Room-Temperature Synthesis of UiO-66 and Thermal Modulation of Densities of Defect Sites. *Chem. Mater.* **2017**, *29*, 1357−1361.
(39) Huang, Y. H.; Lo, W. S.; Kuo, Y. W.; Chen, W. J.; Lin, C. H.; Shieh, F. K. Green and Rapid Synthesis of Zirconium Metal−Organic Frameworks via Mechanochemistry: UiO-66 Analog Nanocrystals Obtained in One Hundred Seconds. *Chem. Commun.* **2017**, *53*, 5818−5821.
(40) Užarević, K.; Wang, T. C.; Moon, S. Y.; Fidelli, A. M.; Hupp, J. T.; Farha, O. K.; Friščić, T. Mechanochemical and Solvent-Free Assembly of Zirconium-Based Metal-Organic Frameworks. *Chem. Commun.* **2016**, *52*, 2133−2136.
(41) Zou, C.; Vagin, S.; Kronast, A.; Rieger, B. Template Mediated and Solvent-Free Route to a Variety of UiO-66 Metal-Organic Frameworks. *RSC Adv.* **2016**, *6*, 102968−102971.
(42) Wu, Q. M.; Wang, X.; Qi, G. D.; Guo, Q.; Pan, S. X.; Meng, X. J.; Xu, J.; Deng, F.; Fan, F. T.; Feng, Z. C.; Li, C.; Maurer, S.; Müller, U.; Xiao, F. S. Sustainable Synthesis of Zeolites without Addition of Both Organotemplates and Solvents. *J. Am. Chem. Soc.* **2014**, *136*, 4019−4025.
(43) Leng, K. Y.; Sun, Y. Y.; Li, X. L.; Sun, S.; Xu, W. Rapid Synthesis of Metal-Organic Frameworks MIL-101(Cr) Without the Addition of Solvent and Hydrofluoric Acid. *Cryst. Growth Des.* **2016**, *16*, 1168−1171.
(44) Jin, Y. Y.; Sun, Q.; Qi, G. D.; Yang, C. G.; Xu, J.; Chen, F.; Meng, X. J.; Deng, F.; Xiao, F. S. Solvent-Free Synthesis of Silicoaluminophosphate Zeolites. *Angew. Chem., Int. Ed.* **2013**, *52*, 9172−9175.
(45) Cavka, J. H.; Jakobsen, S.; Olsbye, U.; Guillou, N.; Lamberti, C.; Bordiga, S.; Lillerud, K. P. A New Zirconium Inorganic Building Brick Forming Metal Organic Frameworks with Exceptional Stability. *J. Am. Chem. Soc.* **2008**, *130*, 13850−13851.
(46) Verpoort, F.; Haemers, T.; Roose, P.; Maes, J. P. Characterization of a Surface Coating Formed from Carboxylic Acid-Based Coolants. *Appl. Spectrosc.* **1999**, *53*, 1528−1534.

DOI: 10.1021/acsami.7b10337
ACS Appl. Mater. Interfaces 2017, 9, 34937−34943

(47) Lausund, K. B.; Nilsen, O. All-Gas-Phase Synthesis of UiO-66 Through Modulated Atomic Layer Deposition. *Nat. Commun.* **2016**, *7*, 13578.
(48) (a) Klet, R. C.; Liu, Y. Y.; Wang, T. C.; Hupp, J. T.; Farha, O. K. Evaluation of Brønsted Acidity and Proton Topology in Zr- and Hf-Based Metal-Organic Frameworks using Potentiometric Acid-Base Titration. *J. Mater. Chem. A* **2016**, *4*, 1479−1485.
(49) Bandosz, T. J.; Laskoski, M.; Mahle, J.; Mogilevsky, G.; Peterson, G. W.; Rossin, J. A.; Wagner, G. W. Reactions of VX, GD, and HD with $Zr(OH)_4$: Near Instantaneous Decontamination of VX. *J. Phys. Chem. C* **2012**, *116*, 11606−11614.
(50) Glover, T. G.; Peterson, G. W.; DeCoste, J. B.; Browe, M. A. Adsorption of Ammonia by Sulfuric Acid Treated Zirconium Hydroxide. *Langmuir* **2012**, *28*, 10478−10487.
(51) Sun, Y. Y.; Prins, R. Hydrodesulfurization of 4,6-Dimethyldibenzothiophene over Noble Metals Supported on Mesoporous Zeolites. *Angew. Chem., Int. Ed.* **2008**, *47*, 8478−8481.
(52) Oyama, S. T.; Zhao, H.; Freund, H. J.; Asakura, K.; Włodarczyk, R.; Sierka, M. Unprecedented Selectivity to the Direct Desulfurization (DDS) Pathway in a Highly Active FeNi Bimetallic Phosphide Catalyst. *J. Catal.* **2012**, *285*, 1−5.
(53) Granadeiro, C. M.; Ribeiro, S. O.; Karmaoui, M.; Valenca, R.; Ribeiro, J. C.; de Castro, B.; Cunha-Silva, L.; Balula, S. S. Production of Ultra-Deep Sulfur-Free Diesels using a Sustainable Catalytic System Based on UiO-66(Zr). *Chem. Commun.* **2015**, *51*, 13818−13821.

DOI: 10.1021/acsami.7b10337
ACS Appl. Mater. Interfaces 2017, 9, 34937−34943